Research Article

Hui Sun, Zichao Que, Huinan Wei, Ao Zhou*, Xuan Peng, Wei Cui*, and Xi Wang

Tunning matrix rheology and mechanical performance of ultra-high performance concrete using cellulose nanofibers

https://doi.org/10.1515/ntrev-2022-0099
received December 31, 2021; accepted March 21, 2022

Abstract: With the growing demand for sustainability and rapid development of nanotechnology, nanocellulose materials extracted from natural plants have attracted great attention. The incorporation of nanocellulose materials leads to a change in viscosity and yield stress on ultra-high performance concrete (UHPC). Rheological parameters affect the mechanical strength and steel fiber distribution of UHPC significantly. Therefore, it is essential to adjust the matrix rheology within an appropriate range through nanocellulose materials. This study aims to propose a novel method to optimize steel fiber distribution and mechanical properties of UHPC by adjusting the matrix rheology with cellulose nanofibers (CNFs) suspensions. The relationship among CNF concentration, steel fiber distribution, and the mechanical properties of UHPC was established. Test results showed that the failure mode of UHPC containing CNFs changed from single cracking to multiple cracking, accompanied by 11–23% enhancement in tensile strength. With the increase of CNF concentrations, the probability density distribution functions of steel fiber orientation showed the trend toward the distribution with a larger inclination. The addition of CNF suspensions effectively reduced the number of steel fibers settling to the bottom of the specimens. Scanning electron microscopy analyses demonstrated that the nanoscale reinforcement by CNFs was conducive to improving the mechanical properties of UHPC.

Keywords: ultra-high performance concrete, matrix rheology, fiber distribution, cellulose nanofiber, tensile performance

1 Introduction

Ultra-high performance concrete (UHPC) is known for its ultra-high compressive strength, high compactness, and good durability. According to the curing method and the type of raw materials, UHPC is classified into two categories, that is, UHPC200 and UHPC800. UHPC200 with a compressive strength ranging from 120 to 230 MPa can meet the strength requirement in most constructions [1]. These excellent properties arise from the large amounts of steel fibers inside the UHPC [1,2]. The incorporated steel fibers effectively bridge the cracks of the matrix, allowing the damaged matrix to continue to carry the load [3–5]. However, the crack-bridging effect of the steel fibers is closely related to the fiber distribution [6–8]. A poor fiber distribution will not only reduce the utilization efficiency of steel fibers but also create aggregation or vacancies inside the UHPC matrix, resulting in internal defects of the material [9–11]. Therefore, it is important to fully consider the influencing factors of the fiber distribution in the optimization of the mechanical properties of UHPC. Numerous studies have shown that matrix rheology has a significant effect on the orientation and uniform dispersion of steel fibers [12,13]. Too high plastic viscosity and yield stress are not conducive to the translation and rotation of steel fibers and adversely affect the mechanical properties of UHPC, while too low plastic

* **Corresponding author: Ao Zhou,** School of Civil and Environmental Engineering, Harbin Institute of Technology, Shenzhen, Shenzhen 518055, China, e-mail: zhouao@hit.edu.cn
* **Corresponding author: Wei Cui,** China Construction Science & Technology Group Co., Ltd. Shenzhen Branch, 518118, China, e-mail: cuiwei@cscec.com
Hui Sun: China Construction Science & Technology Group Co., Ltd., Beijing 100195, China
Zichao Que, Huinan Wei: School of Civil and Environmental Engineering, Harbin Institute of Technology, Shenzhen, Shenzhen 518055, China
Xuan Peng: Department of Mechanical Engineering, Suzhou University of Science and Technology, Suzhou 215009, China
Xi Wang: China Construction Science & Technology Group Co., Ltd. Shenzhen Branch, 518118, China

viscosity and yield stress cause the steel fibers to settle significantly under gravity [14]. Based on the above analysis, it is essential to maintain the rheological properties of the UHPC matrix within an appropriate range to obtain a uniform fiber dispersion and better mechanical properties.

Concrete technology is moving towards sustainability with the increasing demand for green development, in the context of which plant fiber concrete has rapidly emerged [15–17]. Cellulose nanofibers (CNFs) extracted from plants are characterized by low toxicity, low environmental risk, low health risk, and biodegradability [18,19], allowing them to outperform most nanomaterials in terms of sustainability and garner extensive attention from researchers worldwide [20]. The existing literature shows that the incorporation of nanocellulose materials in cementitious composites can significantly improve their mechanical properties [21], such as flexural strength and fracture energies, and increase the degree of cement hydration. The flexural strength of normal concrete with CNFs improved by 169.7% compared to that of concrete without CNFs [22]. CNFs also contribute to the freezing-thawing resistance of normal concrete. The mass loss of concrete with CNFs after 100 freezing-thawing cycles was measured as 0.02%, which was 58 times lower than that of the control group [23]. In view of their hydrophilicity and hygroscopicity, cellulose materials can act as an internal water source for cementitious composites [24,25], reducing the number of microcracks and the autogenous shrinkage during the hydration and curing process [26]. In addition, after being incorporated, cellulose fibers can improve the consistency and uniformity of the fresh mixture and enhance the stability of the mixture due to their flexibility and entanglement. This influence can be regarded as the effect of a viscosity modifying agent (VMA) [27,28].

At present, cellulose materials are mostly used in ordinary and self-consolidating concrete to adjust the plastic viscosity and enhance the stability of concrete [21,22]. However, there are few studies in the literature on the application of CNF as VMA in UHPC. The relationship among CNF concentration, steel fiber distribution, and mechanical properties of UHPC remains uncertain. On the one hand, the effective combination of CNFs and UHPC can not only adjust the rheology of the UHPC matrix but also improve the steel fiber distribution. On the other hand, as a kind of nanofiber, CNFs can work together with steel fibers for multiscale reinforcement of matrix cracks to optimize the mechanical properties of UHPC at low steel fiber contents.

This study aims to reveal the influence of matrix rheology on the mechanical properties of UHPC from the perspective of steel fiber distribution. The rheological properties, mechanical performance, and steel fiber distribution were investigated experimentally. In this study, the rheological properties of the UHPC matrix were adjusted by CNF suspension with various concentrations. The steel fiber distribution was evaluated using X-ray computed tomography (CT) scanning and cross-sectional image processing techniques. The results of this study can provide a basis for the use of CNFs as a VMA for UHPC, highlighting the comprehensive relationship among the CNF concentration, steel fiber distribution, and mechanical properties of UHPC.

2 Experiment program

2.1 Raw materials

The cement used was Ordinary Portland cement (P.O 42.5 R) with a specific surface area of 358.6 m^2/kg in this study. Silica fume (SF) was also utilized and the specific surface area was 21,000 m^2/kg. The chemical compositions of cement and SF were listed in Table 1. Fine aggregate is an important part of UHPC, and its fineness affects the steel fiber distribution in the UHPC matrix. Thus, natural river sand with a maximum particle size of 1.18 mm was used. Two types of fibers were applied in UHPC mixtures, including steel fiber and CNF. Straight steel fiber was used with a diameter of 0.2 mm and a length of 13 mm. The tensile strength and elastic modulus of steel fibers are 2,850 MPa and 210 GPa, respectively. CNF with 300–400 nm in length and 20–50 nm in diameter was

Table 1: Chemical compositions of the cement and SF (wt%)

Compound	CaO	SiO_2	Al_2O_3	Fe_2O_3	MgO	Na_2O	K_2O	SO_3	Loss of ignition
Cement	60.26	15.43	7.99	5.36	1.91	0.34	0.13	0.58	3.53
SF	1.20	92.74	1.12	0.79	0.27	—	0.56	—	2.10

incorporated in UHPC mixtures. A polycarboxylate-based superplasticizer (SP) with a greater than 25% water reduction ratio was added to blend mixtures.

2.2 Mix ratio design

The mixture design of UHPC complied with the modified Andreasen and Andersen packing model [1,3]. The mixture proportions are listed in Table 2. According to previous studies, cellulose products are used to adjust the viscosity of cement-based material at low concentrations [21]. At high concentrations, cellulose materials tend to cause entanglement. For this reason, the suspension concentration range was set from 0.05 to 0.25%. In the table, the label "R" refers to UHPC without a CNF suspension, the number 0.05% in "0.05% CNF" indicates that the mass of CNFs in the prepared suspension accounted for 0.05% of the mass of the cementitious material, and the label "CNF" refers to the UHPC incorporating CNF suspension. The other labels were defined similarly.

2.3 Cellulose nanofiber suspension preparation

Due to its high efficiency, ultrasonic dispersion is considered a promising approach to nanomaterial dispersion [29–31]. An ultrasonic disperser with 250 W in output powder and 20 kHz in standard frequency was utilized to prepare the CNF suspensions in this study. The CNF suspension preparation process is shown in Figure 1. First, the CNFs were sampled according to Table 2. Second, the CNF suspension was pre-dispersed using a magnetic stirrer with the temperature-controlled at 25°C and stirring at a speed of 1,000 rpm for 5 min. After the magnetic stirring, the stirring rotor was removed from the container and the suspension was ultrasonically dispersed using an ultrasonic disperser in work-stop-work mode with a total working time of 15 min and a single working time of 1 min (with the work continuing after stopping for 30 s). The purpose of this procedure was to reduce the heat build-up and water evaporation due to a long ultrasonic dispersion time. The CNF suspension was obtained at the end of ultrasonic dispersion.

2.4 Rheological test

The yield stress and plastic viscosity of the fresh UHPC matrix (without steel fibers) were measured using an RM100 rheometer. First, pre-shear was conducted for 10 s at a rate of 10 s^{-1}, after which the changes in the rheological parameters of the UHPC matrix were measured at 15 different shear rates. In the shearing stage, the shear rate increase from 0 to 50 s^{-1} was divided into 10 stages. After reaching 50 s^{-1}, the shear rate increased from 50 to 100 s^{-1} at increments of 10 s^{-1} every 4 s, and then decreased from 100 to 0 s^{-1} according to the same variation pattern. The rheological testing protocol is shown in Figure 2.

To better describe the nonlinear behavior of UHPC with CNFs, the modified Bingham model was employed to determine the rheological parameters of the UHPC matrix [21,27,32]. The equation is described as follows:

$$\tau = \tau_0 + \mu_p \gamma' + c\gamma'^2, \quad (1)$$

where τ_0 is the yield stress (Pa), μ_p is the plastic viscosity (Pa·s), c is the quadratic coefficient of the modified Bingham model (Pa·s^2), γ' is the shear rate (s^{-1}).

2.5 Mechanical test

The compressive and flexural strength tests were conducted using 40 mm × 40 mm × 160 mm prismatic specimens

Table 2: Mix design of UHPC mixtures in this study (kg/m^3)

Notation	Cement	SF	Sand	Water	SP	Steel fiber	CNFs
R (control)	863	215.7	1078.5	169.5	32.4	156	0
0.05% CNF	863	215.7	1078.5	169.5	32.4	156	0.539
0.10% CNF	863	215.7	1078.5	169.5	32.4	156	1.079
0.15% CNF	863	215.7	1078.5	169.5	32.4	156	1.618
0.20% CNF	863	215.7	1078.5	169.5	32.4	156	2.157
0.25% CNF	863	215.7	1078.5	169.5	32.4	156	2.697

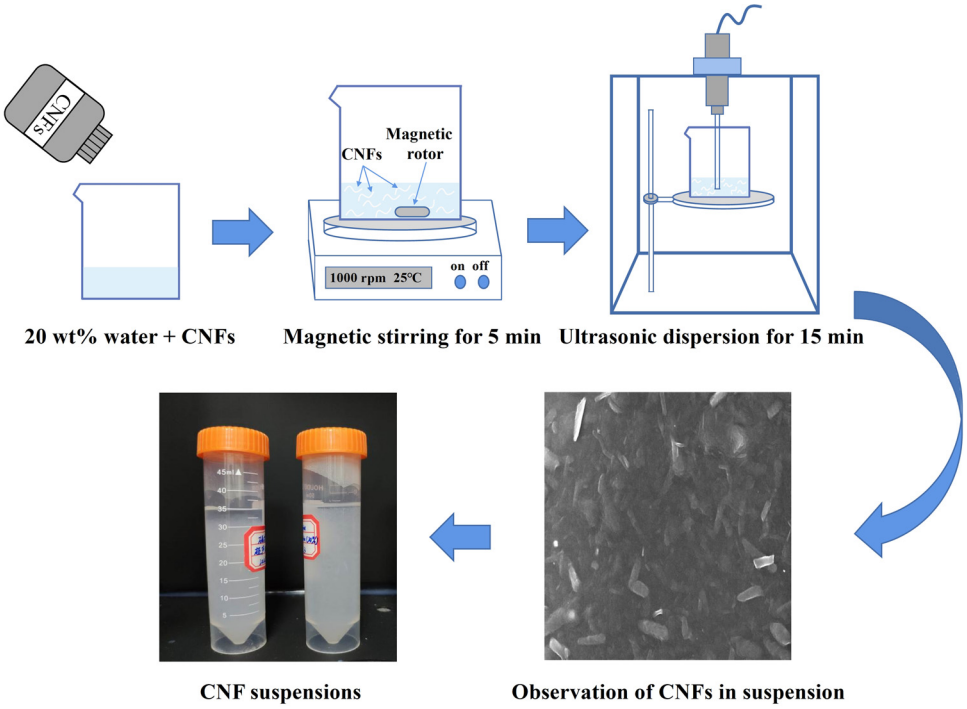

Figure 1: Flow chart of CNF suspension preparation.

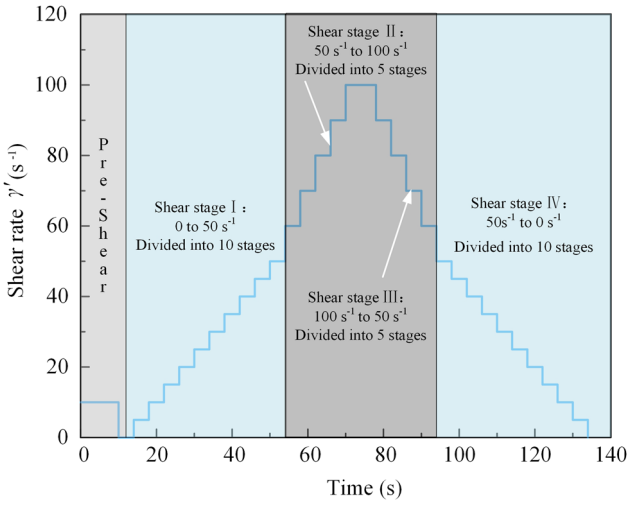

Figure 2: Protocol for rheology test of UHPC matrix.

according to the European standard 196-1:2016. The flexural strength test was carried out using three-point mid-span loading with a span of 100 mm between the supports [33,34]. The flexural toughness test complied with American Society for Testing Materials C1018, and the corresponding value obtained from the integration of load-defection curves up to 6 mm was considered the flexural toughness of specimens. The UHPC tensile strength was measured by a direct tensile test using dog bone-shaped specimens, each of which had a total length of 300 mm, a width of 50 mm, a thickness of 30 mm, and a direct tensile section length of 100 mm. The two ends of each specimen were connected to the direct tensile section by an arc with a radius of 100 mm. Before testing, the clamps for the direct tension were fixed first [35], and then the frame of linear variable differential transformers was installed. During the direct tensile test, the strain contours of each group of specimens in the direct tension direction were measured by the digital image correlation (DIC) technique [36], and the time history of the strain along the crack development path was analyzed.

2.6 Evaluation of steel fiber distribution

In order to quantitatively analyze the distribution characteristics of steel fibers, the distribution characteristics of steel fibers in UHPC were divided into fiber orientation and dispersion. A Tomoscope L 300 microtomography (X-ray CT) with a 260 kV/250 μA tube was employed to obtain the binary images of UHPC specimens. The samples for the X-ray CT scan were taken from the cross-section near the fracture position of tensile specimens after the direct tensile test [37]. 2D slices with pixel sizes of 1,024 × 1,024 were provided for each sample. Based on the obtained CT images, the minor axis, main axis,

number, and sectional areas of the fiber cross-section were recognized by the image processing software [38,39]. The fiber inclination θ paralleled to the direction of tensile load can be calculated by equation (2) [37].

$$\theta = \arccos\left(\frac{d_f}{a}\right), \tag{2}$$

where d_f is the minor axis of fiber cross-section. Since the steel fiber contour on the cross-section of the samples is oval or circular, the measured minor axis of fiber cross-section d_f is the fiber diameter. a is the main axis of fiber cross-section.

The corresponding probability density function $p(\theta)$ of steel fiber inclination can be expressed as follows [13].

$$p(\theta) = \frac{\{\sin\theta\}^{2r-1}\{\cos\theta\}^{2q-1}}{\int_{\theta_{\min}}^{\theta_{\max}}\{\sin\theta\}^{2r-1}\{\cos\theta\}^{2q-1}d\theta}, \tag{3}$$

where r and q are the shape parameters.

Taking the steel fiber number and sectional areas into consideration during the fiber dispersion evaluation, the cross-section of samples was divided into four even rectangular regions. The number and area of fibers in each rectangular part were counted, respectively. The fiber local dispersion coefficient γ_i is given by equation (4).

$$\gamma_i = \frac{n_i \cdot S_i}{\sum_{i=1}^{4} n_i \cdot S_i}, \tag{4}$$

where n_i is the fiber number in the i-th part, and S_i is the fiber sectional area in the i-th part.

3 Results and discussion

3.1 Rheological properties

The CNF suspensions were prepared to improve the matrix rheology of the UHPC. Figure 3 depicts the rheological curves of the UHPC matrix with various concentrations of CNF suspensions. The measured rheological properties of the UHPC matrix with different CNF suspension concentrations are summarized in Table 3. The rheological curves incorporated with CNF suspensions were in good agreement with the modified Bingham model [13].

The comparison of the changes in rheological properties of the UHPC matrix after incorporating CNF suspensions with concentrations of 0.05, 0.10, 0.15, 0.20, and 0.25% showed that five different concentrations of CNF suspensions led to an increase in the yield stress of the

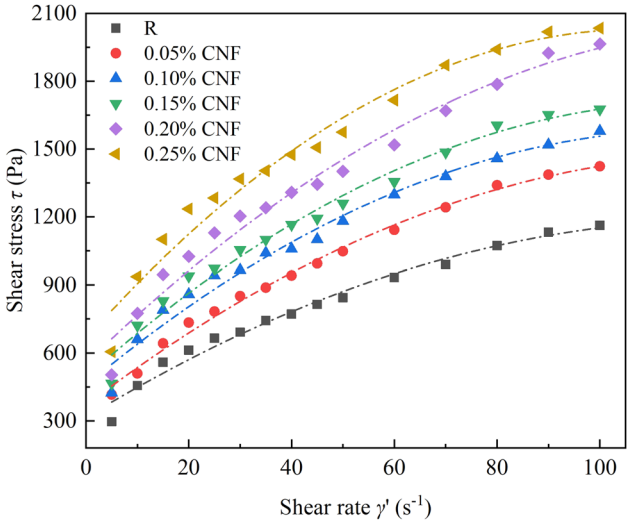

Figure 3: Rheological curves of the UHPC matrix with various concentrations of CNF suspensions.

UHPC matrix from 314.68 Pa to 368.61, 457.20, 492.97, 554.20, and 663.17 Pa, respectively, and plastic viscosity from 13.90 Pa·s to 17.35, 18.97, 20.24, 22.08, and 25.44 Pa·s, respectively. The above results indicate that CNF suspension significantly affected the rheological properties of the UHPC matrix and the influence was greater on the yield stress than plastic viscosity in terms of the variation range. This experimental phenomenon was consistent with the observations by other researchers [13]. Figure 3 also shows that the UHPC matrix containing CNF suspensions exhibited a high viscosity at low shear rates but the apparent viscosity of the matrix decreased as the shear rate continued to increase. Such rheological behavior is called shear thinning. A similar phenomenon has also been reported before [27]. It is found that CNFs have the trend of self-assembly, allowing CNFs to form a network [19,27]. The increase in viscosity when the UHPC was at a low shear rate was attributed to the network formed by CNFs, which means more external force was required to break the CNFs network [40]. When a high shear rate was

Table 3: Rheological parameters of the UHPC matrix

Notation	Plastic viscosity (Pa·s)	Yield stress (Pa)	R^2
R	13.90	314.68	0.982
0.05% CNF	17.35	368.61	0.994
0.10% CNF	18.97	457.20	0.978
0.15% CNF	20.24	492.97	0.980
0.20% CNF	22.08	554.20	0.976
0.25% CNF	25.44	663.17	0.970

adjusted, enough shear force pulverized the CNFs network and the viscosity began to decrease [19,27].

3.2 Mechanical strength

The influence of CNF content on the basic mechanical strength of the UHPC is shown in Figure 4. The incorporation of CNFs had little influence on the compressive strength of UHPC at 28 days. For the compressive performance of UHPC, the existence of steel fiber played a significant role, while CNFs played an insignificant role. The compressive strength of UHPC mainly depends on the aspect ratio and volume ratio of steel fibers. The flexural strength of the UHPC at 28 days was significantly affected by the incorporation of CNFs, showing a trend of first increase and then decrease. As illustrated in Figure 4, the highest flexural strength was measured as 39.17 MPa for 0.15% CNF. Under a CNF suspension concentration of 0.25%, the UHPC had a flexural strength of 31.67 MPa, which was 19.15% lower than that of 0.15% CNF. The reason is that a large number of air voids were difficult to be removed and form pores within the matrix, reducing the flexural strength of UHPC.

3.3 Flexural ductility

Ductility refers to the energy absorption capacity of material during plastic deformation and fracture [41,42], and it is a comprehensive index of ductility and strength. Flexural ductility is one of the important reference indices for evaluating the performance of fiber-reinforced concrete [43]. Figure 5 shows the effect of CNF suspensions with various concentrations on flexural performance. As shown in Figure 5(a), the load-deflection curve of the UHPC was roughly divided into three stages: a pre-crack elastic stage, a crack development stage, and a post-crack softening stage. As illustrated in Figure 5(b), at the pre-crack elastic stage, a linear increase in flexural load with deflection was observed. After the flexural load reached the first cracking load, the UHPC specimens were at the crack development stage and the load increased nonlinearly with deflection. At the post-crack softening stage, the curve exhibited a sudden drop after the peak value, which was attributed to the pullout of steel fibers [11].

Furthermore, the incorporation of CNFs significantly improved the crack-bridging effect of fibers. The calculated results of the flexural toughness of each group of specimens are shown in Figure 5(c). The flexural toughness of UHPC with CNFs tended to increase first and then decrease. The maximum increase in flexural toughness was 66.77% under a CNF suspension concentration of 0.15%, which agreed with the trend of flexural strength of UHPC. The reason is that when the CNF suspension concentration was less than 0.15%, CNFs improved the transition zone of the steel fiber/matrix interface at the nanoscale by reinforcing the UHPC matrix, which effectively bridged the microcracks and formed multi-scale reinforcement with the steel fibers. Therefore, flexural toughness increased with CNF concentrations. However, as the CNF concentration continued to increase, the increase rate of flexural toughness started to decrease. Relative to that of 0.15% CNF, the flexural toughness of 0.20% CNF and 0.25% CNF decreased by 19.62 and 25.80%, respectively but the values were still higher than that of R.

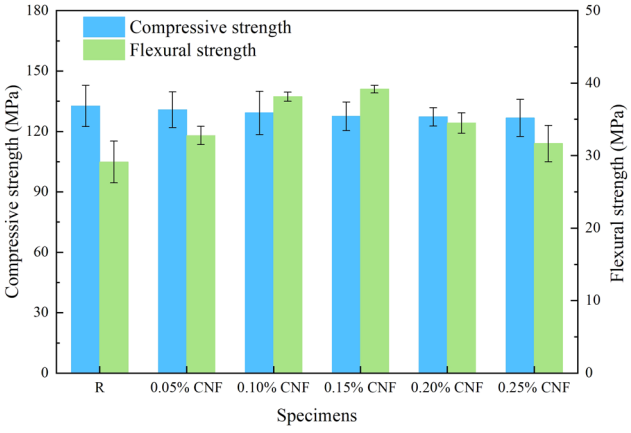

Figure 4: Compressive and flexural strength of UHPC specimens.

3.4 Tensile performance

The stress-strain curves of UHPC with different CNF contents are shown in Figure 6. All the UHPC specimens exhibited strain hardening behavior. In the elastic stage, the tensile stress increased linearly with tensile strain when in the range of 0.02–0.04%. In the strain-hardening stage, the specimen reached the ultimate tensile strength (σ_{pt}) during the process from the first cracking strain (ε_{ft}) to the ultimate tensile strain (ε_{pt}). After this, the stress decreased nonlinearly with the increase in tensile strain in the strain-softening stage. The peak value of

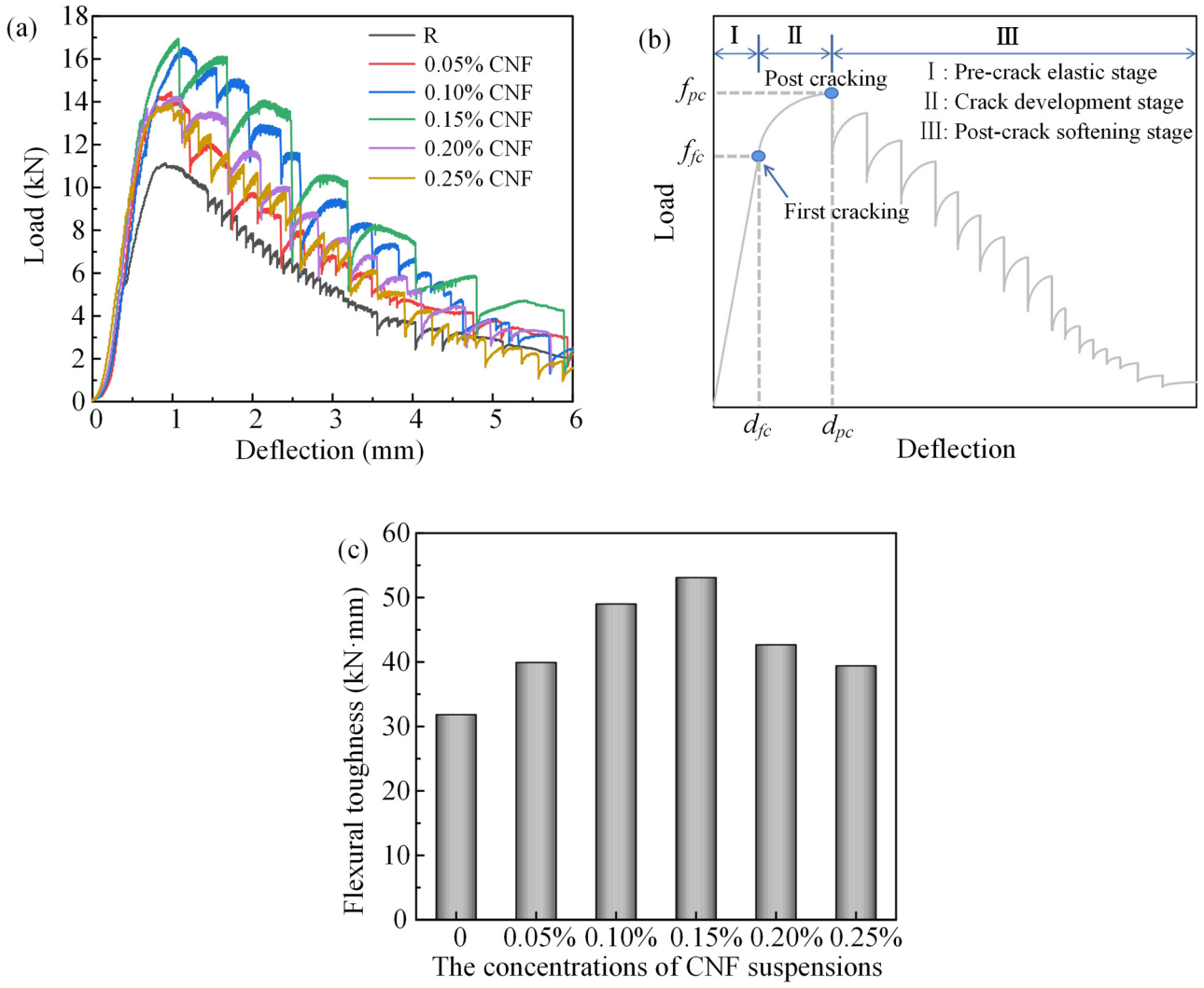

Figure 5: Effect of CNF suspensions with various concentrations on flexural performance: (a) load–deflection curves of UHPC; (b) three typical stages of load-deflection curves; (c) flexural toughness of UHPC.

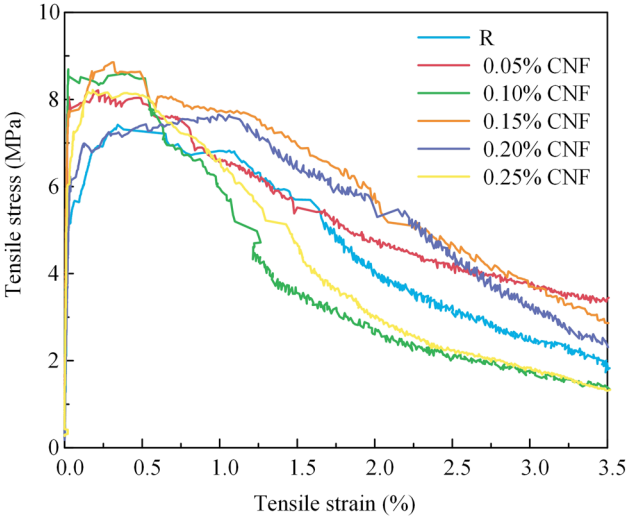

Figure 6: Tensile stress–strain curves of UHPC specimens.

tensile stress increased with the increase in the CNF content. To compare the energy absorption capacity of UHPC during the direct tensile test, the energy absorption before strain softening (G_a) was calculated, which refers to the area of the stress-strain curve up to ε_{pt}.

The results of the direct tensile tests are summarized in Table 4 based on the stress-strain curves of each group of the UHPC specimens. The tensile strength (σ_{pt}) of the UHPC showed a trend of increase first and then decrease with the increase in the CNF suspension concentration. The σ_{pt} of 0.15% CNF was 8.96 MPa, which increased by 23.25% compared to that of the control group. In addition, the incorporation of CNFs had little influence on the ε_{ft} and ε_{pt} UHPC. The first cracking strength (σ_{ft}) and energy absorption before strain softening (G_a) showed a similar trend of first increasing and then decreasing. For

Table 4: Test results of specimens with various concentrations of CNF suspensions

Notation	σ_{pt} (MPa)	ε_{pt} (%)	σ_{ft} (MPa)	ε_{ft} (%)	G_a (kJ/m^3)
R	7.27	0.34	5.11	0.02	21.44
0.05% CNF	8.38	0.31	8.15	0.02	25.54
0.10% CNF	8.44	0.30	8.22	0.03	26.81
0.15% CNF	8.96	0.33	7.59	0.03	26.51
0.20% CNF	8.14	0.31	6.87	0.03	21.83
0.25% CNF	8.10	0.32	6.40	0.03	21.43

0.10% CNF, the σ_{ft} and G_a were 8.22 MPa and 26.81 kJ/m^3, which improved by 60.86 and 25.05%, respectively.

Three typical DIC results of UHPC with different CNF contents are plotted in Figure 7. The strain in the ε_{yy} direction was measured by the DIC technique to reveal the changes in the crack propagation of specimens. When the CNF suspension was not incorporated into UHPC, the control group R tended to have a straight crack propagation path and exhibited a single crack. When the CNF suspension with a concentration of 0.15% was incorporated, the UHPC specimens presented double cracks, and the crack propagation path tended to be tortuous. When the CNF suspension concentration increased to 0.25%, the specimens also showed a failure mode of double cracking and the crack propagation path became more tortuous than that of 0.15% CNF.

Figure 8 shows the timeline of the strain along the crack development path for three typical groups of UHPC. In ascending order, the matrix cracking times were ranked as follows: 0.20%, 0.25%, R, 0.15%, 0.10%, and 0.05%. When the concentration was in the range of 0.05–0.15%, CNFs delayed the cracking time and strain development rate of the matrix. When the concentration increased to 0.20–0.25%, CNFs accelerated the cracking and strain growth rate of the matrix. This is attributed to the fact that when CNF suspension concentration was in the range of 0.05–0.15%, the multiscale reinforcement of the matrix by CNFs and steel fibers played a dominant role, thus delaying the cracking time and strain development rate of the matrix but such an effect decreased with an increase in the suspension concentration. When the suspension concentration increased to 0.25%, the deterioration of the fiber distribution caused by the thickening of the matrix played a dominant role, thus accelerating the cracking and strain development of the matrix.

The scanning electron microscopy (SEM) results showed the following. Significant cracks between the steel

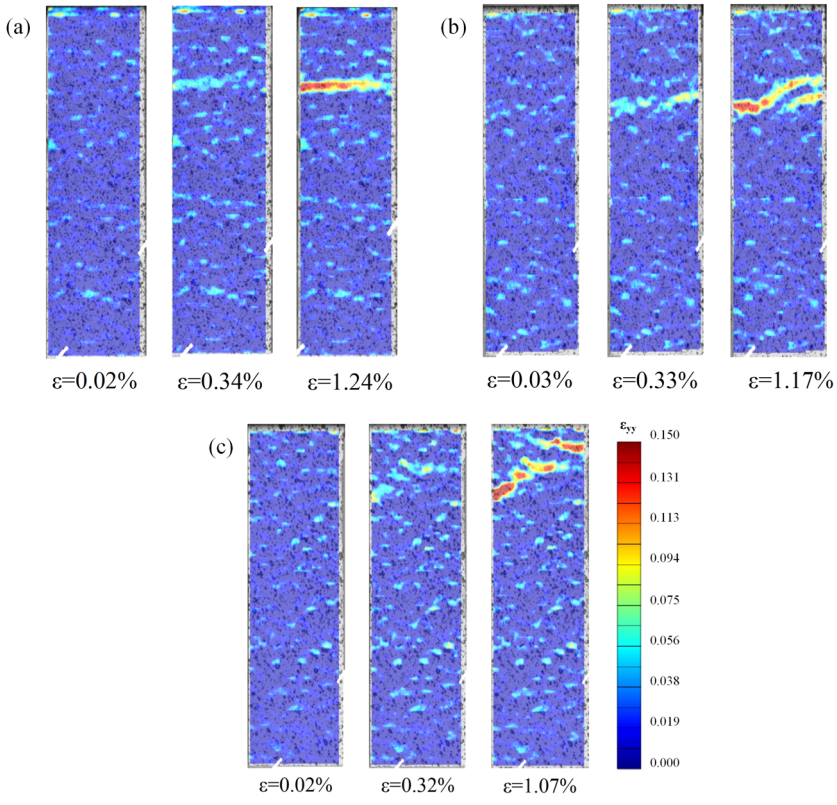

Figure 7: Evolution of the crack during the direct tensile test of (a) R; (b) 0.15% CNF; (c) 0.25% CNF.

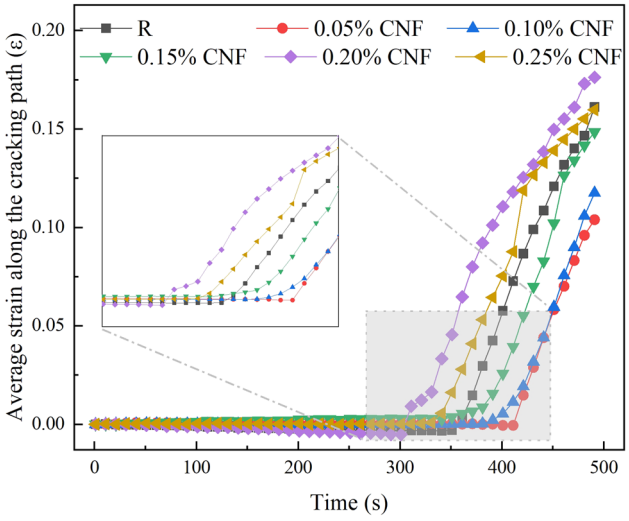

Figure 8: Average strain of specimens with various matrix rheology along the cracking path.

fibers and the UHPC matrix were observed in the control group R, as shown in Figure 9(a). In Figure 9(b), it was observed that the incorporation made the interfacial transition zone (ITZ) between the steel fiber and UHPC matrix denser. This phenomenon coincided with the previous literature [23]. The dense microstructure was attributed to the filling effect of CNFs. In addition, CNFs were hydrophilic and closely bonded with the UHPC matrix to enhance the bonding of various components within UHPC, improving the transition zone of the steel fiber-matrix interface.

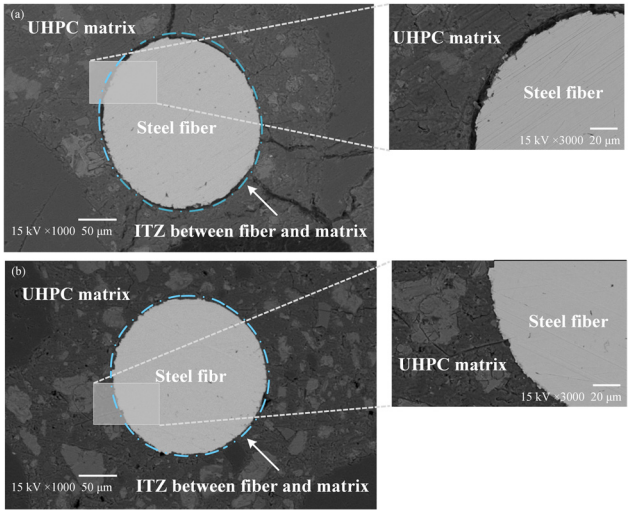

Figure 9: Morphologies of UHPC specimen without CNF and with 0.15% CNF. (a) ITZ between steel fiber and matrix of UHPC without CNF. (b) ITZ between steel fiber and matrix of UHPC with 0.15% CNF.

The role of fibers in fiber-reinforced cement-based materials is to bridge cracks in the matrix and prevent the further development of cracks [44]. Cracks existing in UHPC can be classified into two categories, that is, macrocracks and microcracks. CNFs can effectively inhibit the propagation of microcracks, whereas steel fibers exhibit better performance in the prevention of macrocracks [45]. Figure 10 presents the SEM image of 0.15% CNF. Several fine filaments bridging cracks within the matrix were observed, indicating that CNFs as a type of fiber can effectively bridge macrocracks through nanoscale reinforcement of the matrix. Moreover, CNFs can also interact with hydration products containing hydrogen atoms through the OH^- groups, improving the bonding between CNFs and matrix [46,47]. The above results reveal that the incorporation of CNFs can optimize the mechanical properties of UHPC by enhancing the compactness of ITZ and bridging the cracks within the UHPC matrix.

3.5 Fiber distribution

In an ideal orientation distribution of steel fibers, all the steel fibers are parallel to the longitudinal direction of specimens, resulting in the largest bridging efficiency of fibers [37,39]. To further explore the variation of steel fiber distribution of UHPC after adding CNF suspensions with various concentrations, three groups of specimens (R, 0.15% CNF, and 0.25% CNF) were selected for X-ray CT scanning. The steel fibers' spatial distribution of UHPC is shown in Figure 11. It is worth noting that the distribution density of steel fibers located at the bottom of specimens decreased with the increase of CNF contents, implying that the increased plastic viscosity reduced the number of sinking steel fibers under gravity.

The probability density distribution functions of steel fiber inclination of UHPC specimens with different CNF concentrations are shown in Figure 12. The fiber

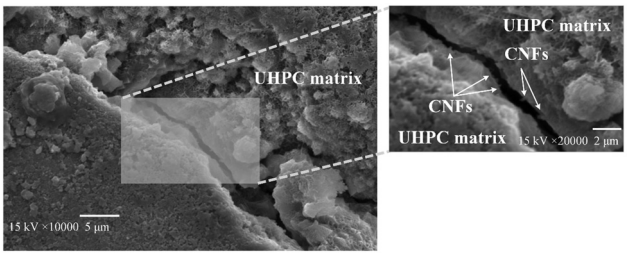

Figure 10: SEM image of 0.15% CNF. The image shows that CNFs bridged the crack within UHPC matrix.

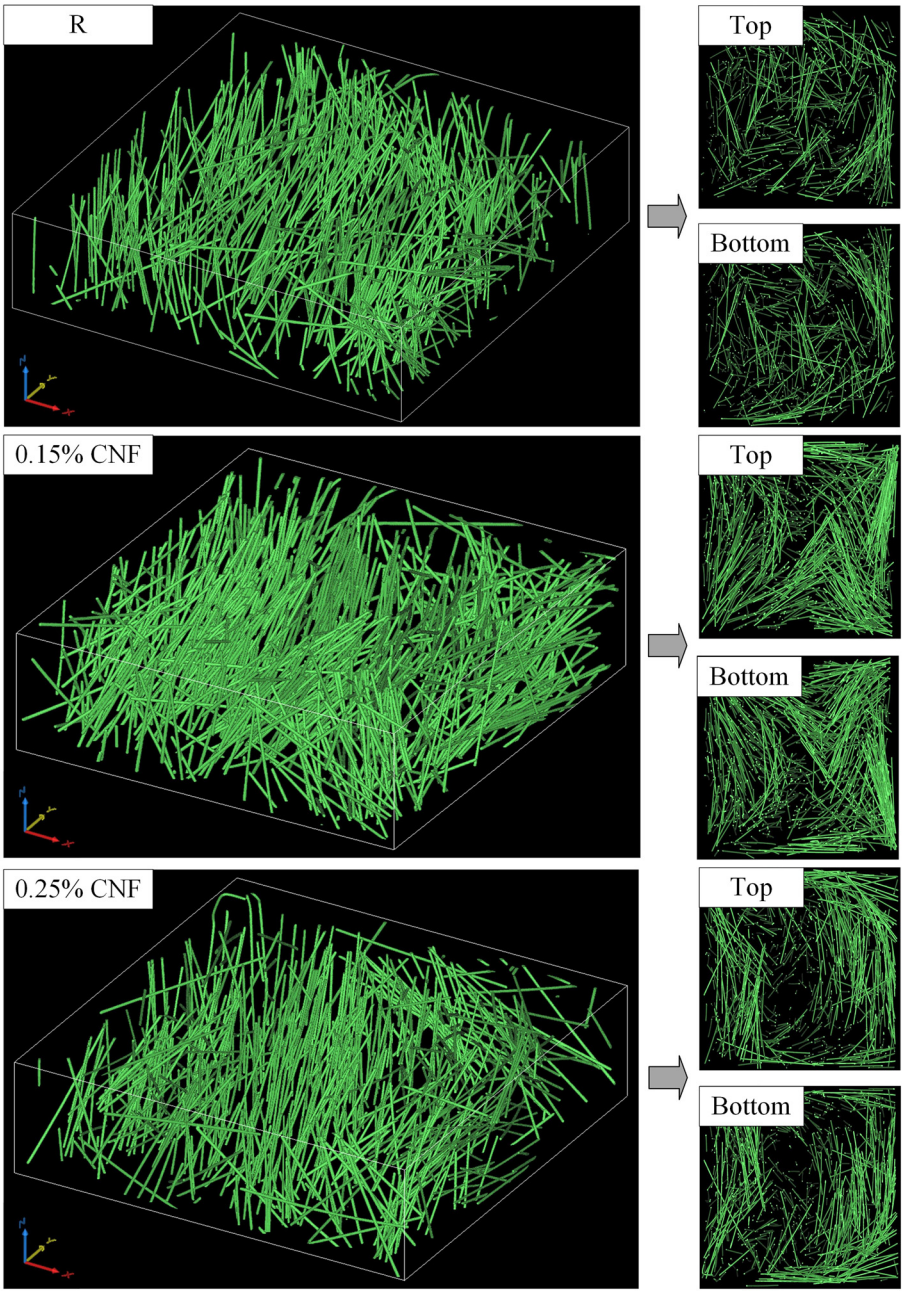

Figure 11: Steel fibers spatial distribution of UHPC specimens with various matrix rheology. The distribution density of steel fibers at the bottom of specimens decreased with the increase in CNF concentrations.

orientation of R and 0.15% CNF specimens tended to be symmetrically distributed, while the fiber orientation of 0.25% CNF specimens tended to have a right-skewed distribution. When the CNF suspension with a concentration of 0.15% was incorporated, the probability of steel fibers in the range of 0.4–0.8 rad had a higher degree of aggregation than that of R. When the CNF suspension concentration increased to 0.25%, the probability density distribution curve of the steel fiber orientation tended to shift toward larger inclinations. The above analyses indicated that CNF suspension with a concentration of less than 0.15% improved the orientation of steel fibers in UHPC to a certain extent. Compared to the control R and 0.15% CNF specimens, when the suspension concentration continued to increase, the thickening of the UHPC matrix was not conducive to the orientation arrangement of steel fibers in UHPC, resulting in an overall shift of the curve of 0.25% CNF specimens toward large inclinations.

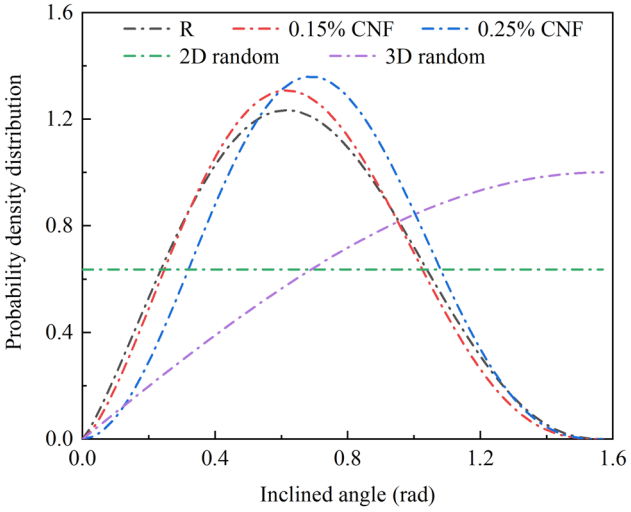

Figure 12: Probability density distribution of steel fiber inclination. The increase of steel fiber distribution probability in the inclined angle interval ranging from 0.4 to 0.8 rad indicates that the orientation has been optimized after adding CNF suspensions.

The changes in the rheological properties of the UHPC matrix affected not only the orientation arrangement but also the uniform dispersion of the steel fibers in UHPC. To further investigate the role of matrix rheology in the local dispersion of steel fibers, the local fiber dispersion coefficient γ_i for each part of the specimens was calculated. Figure 13 shows the steel fiber local distribution on the cutting cross-section of samples. The aggregation and vacancy of steel fibers are distinguished by the depth of blue colors. The γ_i value approaching 0.25 means that steel fibers tend to disperse uniformly. Based on the color depth of different regions of investigated UHPC, it was found that the control group R exhibited significant fiber aggregation at S4. The 0.15% CNF specimens had a consistent fiber dispersion in each region, while the 0.25% CNF specimens showed slight fiber vacancies at S3. Results demonstrated that the incorporation of CNFs suspensions effectively reduced the number of steel fibers sinking to the bottom of specimens under gravity by adjusting the matrix rheology. The effect of CNF suspensions on steel fiber distribution can explain the variation of σ_{ft} and G_a in Section 3.4.

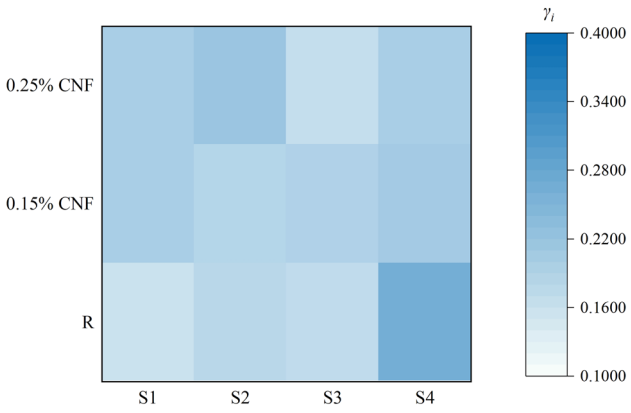

Figure 13: Steel fiber local distribution on the cutting cross-section of UHPC. The aggregation and vacancy of steel fibers are distinguished by the depth of blue colors. The darker color indicates that large amounts of steel fibers are dispersed in the region.

4 Conclusion

In this study, the rheological parameters of UHPC were adjusted by adding CNF suspensions at a low concentration. The compressive strength, flexural strength, and toughness of UHPC containing CNFs were investigated. Tensile strength, energy absorption before strain softening, and timelines of the strain along the cracking path were used to evaluate the tensile performance of UHPC. The morphologies of UHPC containing CNFs and steel fiber spatial distribution were characterized by SEM and CT, respectively. Test results showed that CNF can significantly increase the plastic viscosity and yield stress of UHPC. With the increase in CNF concentration, the flexural strength and toughness of UHPC increased first and then decreased. For UHPC with 0.15% CNF, the corresponding flexural toughness increased by 66.77%. The direct tensile failure mode of the UHPC changed from single cracking to multiple cracking after adding CNFs. CNFs at low concentrations ranging from 0.05 to 0.15% can delay the cracking time of matrix and strain development rate on the cracking path. The microscopic results showed that the addition of the CNF suspension improves the compactness of the internal structure of UHPC, and the CNFs bridge and fill the microcracks of the matrix. The quantitative analyses of the fiber distribution indicate that UHPC with CNFs obtained more uniform steel fiber dispersion, which was attributed to the reduction in the number of steel fibers settling to the bottom of specimens. Owing to the increased viscosity caused by CNF suspensions, the probability density distribution curves of steel fiber orientation were observed to show the trend toward the distribution with a larger inclination.

Funding information: This work was supported by the National Natural Science Foundation of China (Grant Number: 51908167); Key Research and Development Program of Guangdong Province (Grant Number: 2019B1111 07001); and Shenzhen Science and Technology Programs (Grant Number: RCBS20200714114819352).

Author contributions: All authors have accepted responsibility for the entire content of this manuscript and approved its submission.

Conflict of interest: The authors declare that they have no conflict of interest.

References

[1] Liu TJ, Wei HN, Zou DJ, Zhou A, Jian HS. Utilization of waste cathode ray tube funnel glass for ultra-high performance concrete. J Clean Prod. 2020;249:119333.

[2] Kang ST, Kim JK. The relation between fiber orientation and tensile behavior in an ultra high performance fiber reinforced cementitious composites (UHPFRCC). Cem Concr Res. 2011;41(10):1001–14.

[3] Liu TJ, Wei HN, Zhou A, Zou DJ, Jian HS. Multiscale investigation on tensile properties of ultra-high performance concrete with silane coupling agent modified steel fibers. Cem Concr Compos. 2020;111:103638.

[4] Zhou A, Wei HN, Liu TJ, Zou DJ, Li Y, Qin RY. Interfacial technology for enhancement in steel fiber reinforced cementitious composite from nano to macroscale. Nanotechnol Rev. 2021;10(1):636–52.

[5] Zhou A, Yu Z, Wei H, Tam LH, Liu T, Zou D. Understanding the toughening mechanism of silane coupling agents in the interfacial bonding in steel fiber-reinforced cementitious composites. Acs Appl Mater Inter. 2020;12(39):44163–71.

[6] Abrishambaf A, Barros JAO, Cunha VMCF. Relation between fibre distribution and post-cracking behaviour in steel fibre reinforced self-compacting concrete panels. Cem Concr Res. 2013;51:57–66.

[7] Alberti MG, Enfedaque A, Galvez JC. On the prediction of the orientation factor and fibre distribution of steel and macro-synthetic fibres for fibre-reinforced concrete. Cem Concr Compos. 2017;77:29–48.

[8] Ruan T, Poursaee A. Fiber-distribution assessment in steel fiber–reinforced UHPC using conventional imaging, X-Ray CT scan, and concrete electrical conductivity. J Mater Civ Eng. 2019;31(8):04019133.

[9] Kang ST, Lee BY, Kim JK, Kim YY. The effect of fibre distribution characteristics on the flexural strength of steel fibre-reinforced ultra high strength concrete. Constr Build Mater. 2011;25(5):2450–7.

[10] Mobasher B, Stang H, Shah SP. Microcracking in fiber reinforced-concrete. Cem Concr Res. 1990;20(5):65–76.

[11] Wei HN, Liu TJ, Zhou A, Zou DJ, Liu Y. Multiscale insights on enhancing tensile properties of ultra-high performance cementitious composite with hybrid steel and polymeric fibers. J Mater Res Technol. 2021;14:743–53.

[12] Li M, Li VC. Rheology, fiber dispersion, and robust properties of engineered cementitious composites. Mater Struct. 2012;46(3):405–20.

[13] Teng L, Meng WN, Khayat KH. Rheology control of ultra-high-performance concrete made with different fiber contents. Cem Concr Res. 2020;138:106222.

[14] Ozyurt N, Mason TO, Shah SP. Correlation of fiber dispersion, rheology and mechanical performance of FRCs. Cem Concr Compos. 2007;29(2):70–9.

[15] Wei HN, Zhou A, Liu TJ, Zou DJ, Jian HS. Dynamic and environmental performance of eco-friendly ultra-high performance concrete containing waste cathode ray tube glass as a substitution of river sand. Resour Conserv Recycl. 2020;162:105021.

[16] Zhou A, Qiu QW, Chow CL, Lau D. Interfacial performance of aramid, basalt and carbon fiber reinforced polymer bonded concrete exposed to high temperature. Compos Part A Appl S. 2020;131:105802.

[17] Liu TJ, Wang ZZ, Zou DJ, Zhou A, Du JZ. Strength enhancement of recycled aggregate pervious concrete using a cement paste redistribution method. Cem Concr Res. 2019;122:72–82.

[18] Mao L, Hu S, Gao Y, Wang L, Zhao W, Fu L, et al. Cellulose hydrogel skeleton by extrusion 3D printing of solution. Nanotechnol Rev. 2020;9(1):345–53.

[19] Moon RJ, Martini A, Nairn J, Simonsen J, Youngblood J. Cellulose nanomaterials review: structure, properties and nanocomposites. Chem Soc Rev. 2011;40(7):3941–94.

[20] Radakisnin R, Majid MSA, Jamir MRM, Tahir MFM, Meng CE, Al Alshahrani H. Physical, thermal, and mechanical properties of highly porous polylactic acid/cellulose nanofibre scaffolds prepared by salt leaching technique. Nanotechnol Rev. 2021;10(1):1469–83.

[21] Hisseine OA, Omran AF, Tagnit-Hamou A. Influence of cellulose filaments on cement paste and concrete. J Mater Civ Eng. 2018;30(6):04018109.

[22] Cengiz A, Kaya M, Bayramgil NP. Flexural stress enhancement of concrete by incorporation of algal cellulose nanofibers. Constr Build Mater. 2017;149:289–95.

[23] Barnat-Hunek D, Szymanska-Chargot M, Jarosz-Hadam M, Lagod G. Effect of cellulose nanofibrils and nanocrystals on physical properties of concrete. Constr Build Mater. 2019;223:1–11.

[24] Fu L, Ma Q, Liao K, An J, Bai J, He Y. Application of pickering emulsion in oil drilling and production. Nanotechnol Rev. 2021;11(1):26–39.

[25] Sainorudin MH, Abdullah NA, Asmal Rani MS, Mohammad M, Mahizan M, Shadan N, et al. Structural characterization of microcrystalline and nanocrystalline cellulose from Ananas comosus L. leaves: Cytocompatibility and molecular docking studies. Nanotechnol Rev. 2021;10(1):793–806.

[26] Wang W, Shen A, Lyu Z, He Z, Nguyen KTQ. Fresh and rheological characteristics of fiber reinforced concrete – A review. Constr Build Mater. 2021;296:123734.

[27] Hisseine OA, Basic N, Omran AF, Tagnit-Hamou A. Feasibility of using cellulose filaments as a viscosity modifying agent in self-consolidating concrete. Cem Concr Compos. 2018;94:327–40.

[28] Bessaies-Bey H, Khayat KH, Palacios M, Schmidt W, Roussel N. Viscosity modifying agents: Key components of advanced cement-based materials with adapted rheology. Cem Concr Res. 2022;152:106646.

[29] Girard M, Vidal D, Bertrand F, Tavares JR, Heuzey MC. Evidence-based guidelines for the ultrasonic dispersion of cellulose nanocrystals. Ultrason Sonochem. 2021;71:105378.

[30] Parveen S, Rana S, Ferreira S, Filho A, Fangueiro R. Ultrasonic dispersion of micro crystalline cellulose for developing

cementitious composites with excellent strength and stiffness. Ind Crop Prod. 2018;122:156–65.
[31] Qin RY, Zhou A, Yu ZC, Wang Q, Lau D. Role of carbon nanotube in reinforcing cementitious materials: An experimental and coarse-grained molecular dynamics study. Cem Concr Res. 2021;147:106517.
[32] Güneyisi E, Gesoglu M, Naji N, İpek S. Evaluation of the rheological behavior of fresh self-compacting rubberized concrete by using the Herschel–Bulkley and modified Bingham models. Arch Civ Mech Eng. 2016;16(1):9–19.
[33] Zhou A, Zhang WJ, Wei HN, Liu TJ, Zou DJ, Guo HH. A novel approach for recycling engineering sediment waste as sustainable supplementary cementitious materials. Resour Conserv Recycl. 2021;167:105435.
[34] Chen ZY, Li WT, Yu QQ. Characterization of damage and healing of cement matrices based on fly ash under repeated loading. J Mater Civ Eng. 2021;33(1):04020408.
[35] Zhou A, Qin RY, Chow CL, Lau D. Bond integrity of aramid, basalt and carbon fiber reinforced polymer bonded wood composites at elevated temperature. Compos Struct. 2020;245:112342.
[36] Wu C, Chen C, Cheeseman C. Size Effects on the Mechanical properties of 3D printed plaster and PLA parts. J Mater Civ Eng. 2021;33(7):04021152.
[37] Huang HH, Gao XJ, Li LS, Wang H. Improvement effect of steel fiber orientation control on mechanical performance of UHPC. Constr Build Mater. 2018;188:709–21.
[38] Huang HH, Gao XJ, Zhang AL. Numerical simulation and visualization of motion and orientation of steel fibers in UHPC under controlling flow condition. Constr Build Mater. 2019;199:624–36.
[39] Ding C, Guo LP, Chen B. Orientation distribution of polyvinyl alcohol fibers and its influence on bridging capacity and mechanical performances for high ductility cementitious composites. Constr Build Mater. 2020;247:118491.
[40] Cao Y, Zavaterri P, Youngblood J, Moon R, Weiss J. The influence of cellulose nanocrystal additions on the performance of cement paste. Cem Concr Compos. 2015;56:73–83.
[41] Wang YL, Cai GC, Larbi AS, Waldmann D, Tsavdaridis KD, Ran JH. Monotonic axial compressive behaviour and confinement mechanism of square CFRP-steel tube confined concrete. Eng Struct. 2020;217:110802.
[42] Wang YL, Chen GP, Wan BL, Han BG, Ran JH. Axial compressive behavior and confinement mechanism of circular FRP-steel tubed concrete stub columns. Compos Struct. 2021;256:113082.
[43] Zhou Y, Gao H, Hu Z, Qiu Y, Guo M, Huang X, et al. Ductile, durable, and reliable alternative to FRP bars for reinforcing seawater sea-sand recycled concrete beams: steel/FRP composite bars. Constr Build Mater. 2021;269:121264.
[44] Chun B, Yoo DY. Hybrid effect of macro and micro steel fibers on the pullout and tensile behaviors of ultra-high-performance concrete. Compos Part B-Eng. 2019;162:344–60.
[45] Larsen IL, Thorstensen RT. The influence of steel fibres on compressive and tensile strength of ultra high performance concrete: A review. Constr Build Mater. 2020;256:119459.
[46] Hisseine OA, Wilson W, Sorelli L, Tolnai B, Tagnit-Hamou A. Nanocellulose for improved concrete performance: A macro-to-micro investigation for disclosing the effects of cellulose filaments on strength of cement systems. Constr Build Mater. 2019;206:84–96.
[47] Gómez Hoyos C, Cristia E, Vázquez A. Effect of cellulose microcrystalline particles on properties of cement based composites. Mater Des. 2013;51:810–8.